Q. J. R. Meteorol. Soc. (2002), **128**, pp. 2335–2347 doi: 10.1256/qj.01.53

Comparison of an axisymmetric hurricane model with the corresponding slab-symmetric ITCZ model

By WOLFGANG ULRICH[1], ROGER K. SMITH[1]* and NGUYEN CHI MAI[2]

[1]*University of Munich, Germany*

[2]*National Centre for Hydrometeorological Forecasting, Vietnam*

(Received 29 March 2001; revised 4 March 2002)

SUMMARY

We examine the difference between the evolution of a hurricane-like vortex in an axisymmetric model and that of an intertropical convergence-zone-like disturbance in a slab-symmetric model, starting from an initial disturbance with the same lateral structure. The main calculations are carried out using a hurricane model similar to that formulated by DeMaria and Pickle (1988), supplemented by a few calculations using a recently developed model by Nguyen *et al.* (2002). We show that, although the two flow configurations have many similarities, the slab-symmetric model does not provide a dynamical surrogate for the hurricane. The main difference can be attributed to a geometrical factor in the formula for the conservation of absolute angular momentum in the axisymmetric model, which for an inward-moving air parcel permits much larger tangential wind speeds to be attained than in the slab-symmetric model. As a result, the sea-surface latent-heat flux, which is wind-speed dependent, is much larger in the axisymmetric model, providing a larger energy supply to the growing disturbance per unit area than in the slab-symmetric case. A further geometrical effect is that for the same inflow velocity profile in the boundary layer, there is larger convergence in the axisymmetric model. Because this convergence determines the deep cumulus mass flux in the DeMaria and Pickle model, the cumulus heating is larger in the axisymmetric configuration. The non-development of the slab-symmetric perturbation is a feature also of calculations using the Nguyen *et al.* (2002) model, even though two of the closures on the deep-cumulus mass flux used do not depend on the mass convergence in the boundary layer. A few numerical details of the main model are described, including the method of solution, which differs from that used by DeMaria and Pickle (1988).

KEYWORDS: Convective parametrization Hurricanes Tropical cyclones Typhoons

1. INTRODUCTION

In a classical but now controversial paper, Charney and Eliassen (1964) proposed a mechanism for tropical-cyclone intensification which they called conditional instability of the second kind (CISK). The mechanism involved a representation of deep cumulus clouds in which the latent heating is proportional to the low-level moisture convergence in the boundary layer. The basic idea is that increased boundary-layer convergence leads to increased cumulus heating, which in turn leads to increased buoyancy in the vortex. The increased buoyancy leads to enhanced convergence, which in turn increases the vortex strength leading to increased boundary-layer convergence, and so on. Ooyama (1982) stressed that the buoyancy-induced convergence must occur above the boundary layer for vortex intensification. In a subsequent paper to that with Eliassen, Charney (1973) presented a two-dimensional, slab-symmetric version of the model, which might be conceived as a model for the intertropical convergence zone (ITCZ). Over the years there has been an enormous amount of literature on the CISK mechanism and at times it has come under heavy criticism (for recent reviews see Emanuel *et al.* 1994; Ooyama 1997; Smith 1997). However, irrespective of the particular parametrization scheme used, it is pertinent to ask to what extent the axisymmetric and slab-symmetric paradigms are dynamically equivalent. Is the fact that zonally aligned horizontal shear layers such as the ITCZ are not observed to have the intensity of tropical cyclones an indication that they would be unstable to three-dimensional perturbations (possibly leading to tropical-cyclone formation), or is there a difference in the maximum possible intensity

* Corresponding author: Meteorological Institute, University of Munich, Theresienstr. 37, 80333 Munich, Germany. e-mail: roger@meteo.physik.uni-muenchen .de

of such systems on account of the difference in geometry? If the latter were not the case, one might be able to use the slab-symmetric model as a dynamical surrogate for exploring at least some aspects of tropical cyclones with a consequent simplification of the mathematics. We explore this question here using a slightly modified form of the axisymmetric hurricane model formulated by DeMaria and Pickle (1988, henceforth referred to as DP88) and its slab-symmetric equivalent as a basis. We refer to this as model-1. The DP88 model is based on the model formulated by Ooyama (1969), but the governing equations for a compressible fluid are discretized vertically by three layers of air with uniform potential temperature instead of three homogeneous layers of uniform density as used by Ooyama. This change facilitates the representation of thermodynamic processes.

A limitation of the convection scheme used in the Ooyama model is the closure on the deep-cumulus mass flux, which is set proportional to the rate of mass convergence in the boundary layer. For this reason we have carried out similar calculations to those above using the minimal axisymmetric hurricane model recently developed by Nguyen *et al.* (2002) and its slab-symmetric counterpart. This model, which we refer to as model-2, has three layers also, but is formulated in σ-coordinates and has a fully integrated representation of moist processes. In particular, it has a mass-flux scheme to parametrize deep cumulus convection and the option to use one of three different closures for the deep-cumulus mass flux. In two of these closures, the one suggested by Arakawa (1969) and the other used by Emanuel (1995), the cloud-base mass flux is determined independently of the mass convergence in the boundary layer, while the third is similar to the one suggested by Ooyama and that used in model-1.

2. The numerical model

Model-1 consists of three layers of air of uniform potential temperature, the lowest layer (layer-1) is the surface boundary layer and the uppermost layer (layer-3) the outflow layer. The configuration is shown in Fig. 1. The formulation differs only slightly from that used by DP88 (see below), but the solution method is based on finite differences rather than the spectral method. Prognostic equations are solved for the radial and tangential wind components averaged over the depths of each layer and for the depths of these layers. The governing equations, Eqs. (2.36)–(2.38) of DP88, are similar to those derived by Ooyama (1969), but there is an extra term in the pressure-gradient force, and the rate of change of boundary-layer thickness is calculated from $(\partial h_1/\partial t) = -u_1(\partial h_1/\partial r)$, because other terms in Eq. (2.38) of DP88 are zero or cancel. Here h_1 is the deviation of the boundary-layer thickness from its initial value H_1, u_1 is the radial wind component in the boundary layer, r is the radius and t the time. If h_1 were *initially* constant, the boundary-layer thickness would remain constant. Some minor changes to the original DP88 model formulation are adopted from Shapiro (1992); in particular, the surface drag coefficient, C_D, and evaporation coefficient, C_E, are taken to be equal and a function of the wind speed in layer-1. Other changes are detailed in the appendix.

No sensible-heat flux from the surface is allowed in an isentropic model, whereupon the Montgomery stream function in the boundary layer must be evaluated according to $M_1 = \theta_1 \pi_{1/2}$ (recall that M and θ are uniform in the vertical within a layer) and not from $M_1 = c_p T_s$. Here θ_1 is the potential temperature in layer-1, π is the Exner function, defined by $(p/p^*)^\kappa$, where p is the pressure and $p^* = 1000$ mb, c_p is the specific heat capacity of air at constant pressure and T_s is the sea surface temperature. The subscript $1/2$ refers to the interface level where the variable is stored, see Fig. 1.

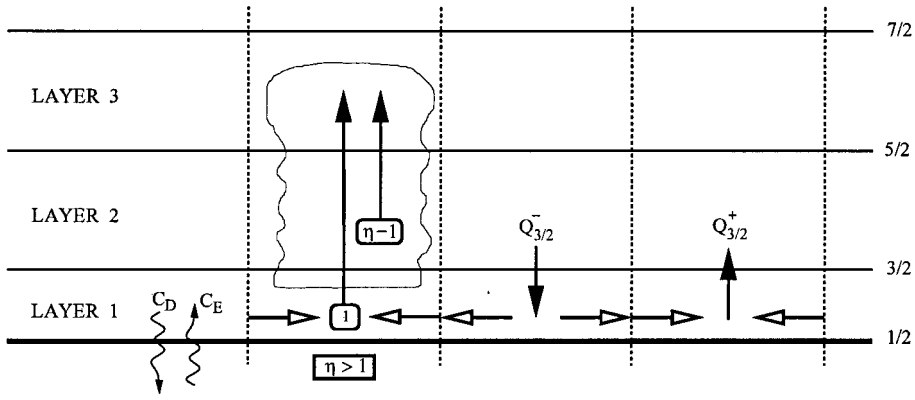

Figure 1. The vertical structure and representation of deep convection in the isentropic model. Deep convection (indicated by the cloud outline) occurs in vertical grid columns (delineated by vertical dashed lines) where there is convective instability ($\eta > 1$) and where there is boundary-layer convergence (indicated by convergent arrows). In such columns, for each unit of mass that ascends from the boundary layer to the middle layer, $\eta - 1$ units are entrained from the middle layer and η units enter the top layer. For columns with boundary-layer divergence there is a mass flux proportional to $Q^-_{3/2}$ from layer-2 into layer-1. Boundary-layer convergence in regions where $\eta < 1$ leads to a mass flux into the middle layer at a rate proportional to $Q^+_{3/2}$.

The value $M_1 = \theta_1 \pi_{1/2}$ is used also for the calculation of the moist static energy in the boundary layer, $\Lambda_1 = M_1 + Lq_1$, and not the procedure proposed by DP88 in their Eq. (3.16). Here q_1 is the water-vapour mixing ratio in the boundary layer and L is the latent heat of vapourization.

The representation of deep convection is also illustrated in Fig. 1. Deep convection occurs where there is convective instability, i.e. where Λ_1 exceeds the saturation moist static energy in the upper layer, Λ^*_3, *and* where there is boundary-layer convergence. In such columns, for each unit of mass that ascends from the boundary layer to the middle layer, $\eta - 1$ units are entrained from the middle layer and η units enter the top layer. The amount of entrainment $(\eta - 1)$ is proportional to the degree of convective instability in a column*, i.e. to $(\Lambda_1 - \Lambda^*_3)$. Mass transfer from the middle layer to the upper layer leads to a thickening of the upper layer and a thinning of the middle layer and is analogous to buoyancy production in a model formulated in height coordinates. In our formulation, deep convection is not allowed for $\eta < 1$. In such regions there is a mass flux from the boundary layer and the middle layer proportional to the diabatic heating rate, $Q^+_{3/2}$, at the interface 3/2, and a mass flux in the other direction proportional to the diabatic cooling rate, $Q^-_{3/2}$, at this level. Other aspects of the model are described in the appendix.

The two-dimensional, slab-symmetric version of the model is obtained by replacing the radial coordinate, r, by the lateral coordinate, x, and derivative terms of the form $(1/r)(\partial \mathcal{F}/\partial r)$ by $\partial \mathcal{F}/\partial x$, where $\mathcal{F}$ is any dependent variable. In the azimuthal- and radial-momentum equations the centrifugal acceleration term and its counterpart are omitted also.

3. THE CALCULATIONS

The radial profile of the initial vortex is that used by Smith *et al.* (1990) with a maximum tangential wind speed of 15 m s^{-1} at a radius of 100 km. The formula is

* Actually $\eta = 1 + (\Lambda_1 - \Lambda^*_3)/(\Lambda^*_3 - \Lambda_2)$.

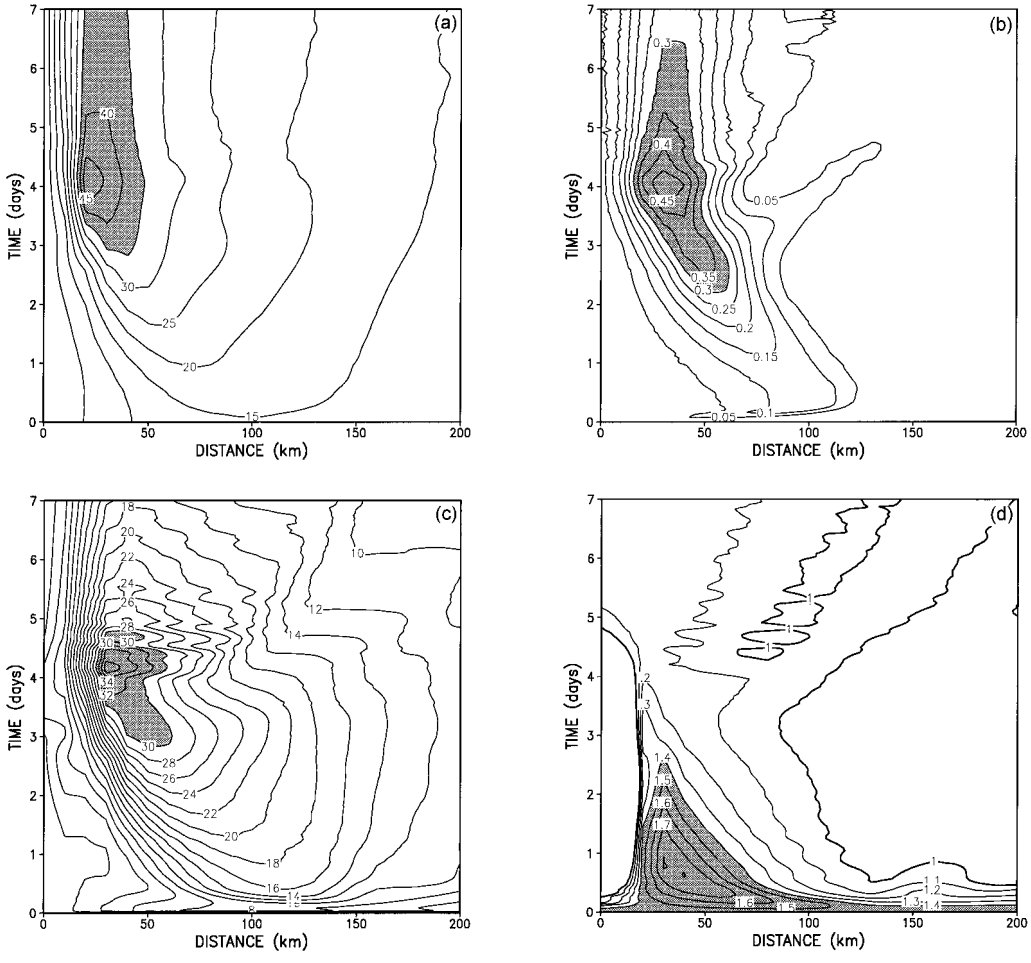

Figure 2. Time–radial plots showing vortex evolution in the axisymmetric case. (a) Isotachs of azimuthal wind speed. Contour interval is 5 m s^{-1} with values larger than 35 m s^{-1} shaded. (b) Isotachs of $Q_{3/2}^{+}$, which is proportional to the mass flux from the boundary layer to the middle layer. Contour interval is 0.05 m s^{-1} with values larger than 0.3 m s^{-1} shaded. (c) Isopleths of moisture flux from the ocean. Contour interval is 2 g $kg^{-1}d^{-1}$ with values larger than 30 g $kg^{-1}d^{-1}$ shaded. (d) Isopleths of the convection parameter, η. Contour interval is 0.1 units with values larger than 1.4 shaded. The degree of convective instability is proportional to $\eta - 1$.

given in the appendix. We carried out two calculations differing only in that one is axisymmetric and the other slab symmetric. The axisymmetric version is initialized with the radial-wind profile in gradient wind balance, whereas the slab-symmetric version is initialized with the same lateral tangential-wind profile in geostrophic balance.

4. RESULTS

Figure 2 shows time–radius plots of the isotachs of azimuthal wind speed in the middle layer and of the vertical velocity at the top of the boundary layer, as well as the isopleths of surface moisture flux and η for the axisymmetric calculation. The corresponding plots for the slab-symmetric calculation are shown in Fig. 3.

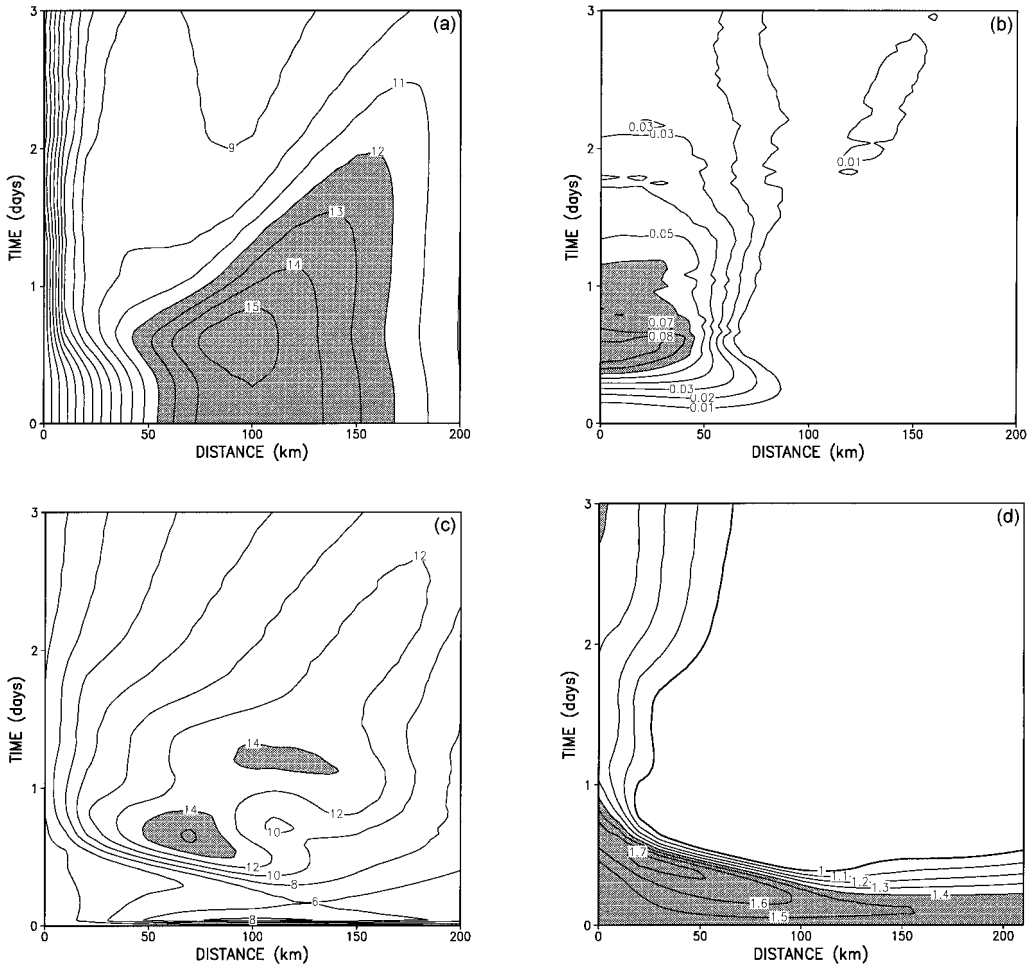

Figure 3. Analogous plots to those in Fig. 2 for the slab-symmetric case. (a) Isotachs of azimuthal (along the intertropical convergence zone) wind speed. Contour interval is 1 m s^{-1} with values larger than 10 m s^{-1} shaded. (b) Isotachs of $Q^{+}_{3/2}$. Contour interval is 0.01 m s^{-1} with values larger than 0.06 m s^{-1} shaded. (c) Isopleths of moisture flux from the ocean. Contour interval is 2 g $kg^{-1}d^{-1}$ with values larger than 14 g $kg^{-1}d^{-1}$ shaded. (d) Isopleths of the convection parameter, η. Contour interval is 0.1 units with values larger than 1.4 shaded. The degree of convective instability is proportional to $\eta - 1$.

(*a*) *Time evolution in the axisymmetric case*

The isotachs of azimuthal wind (Fig. 2(a)) show that the vortex steadily strengthens, reaching its maximum intensity of more than 45 m s^{-1} after 4 days, during which time the radius of maximum winds contracts from 100 km to about 30 km. Beyond 4 days the vortex slowly broadens and the azimuthal wind speed gradually decays. The strengthening of the vortex is accompanied by increased boundary-layer convergence, which is manifested in an increased mass flux through the top of the layer, proportional to $Q^{+}_{3/2}$ (Fig. 2(b)). The increasing boundary-layer wind speeds lead to an increase in the moisture flux from the ocean (Fig. 2(c)), which in turn raises the degree of convective instability, characterized by the magnitude of η (Fig. 2(d)). At the initial time η has a magnitude of 1.4. As the vortex matures, the mass transport from the middle layer to the top layer, which is proportional to $\eta Q^{+}_{3/2}$, causes the top layer to deepen at the expense

of the middle layer. This corresponds with a stabilization of the flow and the values of η progressively decline.

(*b*) *Time evolution in the slab-symmetric case*

The disturbance in the slab-symmetric configuration intensifies only very slightly during the first 15 h and thereafter it steadily decays (Fig. 3(a)). The mass flux out of the boundary layer is much weaker in this case (cf. Figs. 2(b) and 3(b)) as is the surface moisture flux (cf. Figs. 2(c) and 3(c)). Despite the weaker surface flux, the degree of convective instability still increases at early times (cf. Figs. 2(d) and 3(d) and note that the scales along the abscissa and ordinate are different), but because the convergence in the boundary layer is weaker, the horizontal gradient of η is less than in the axisymmetric case. In turn, the weaker gradient of η is analogous to a weaker gradient of convective heating, which acting alone would lead to a weaker vertical circulation than in the axisymmetric case. The vertical circulation is necessary for the intensification of the disturbance.

(*c*) *Intermediate cases*

Two geometrical factors, the conservation of absolute angular momentum rather than linear momentum, and the axisymmetric form of the boundary-layer convergence to evaluate the mass transport rather than the Cartesian form, appear to explain the differences in the evolution. To investigate the separate importance of each contribution, we performed further experiments as follows. The nonlinear terms of the axisymmetric version of DP88 (Eqs. (2.36) and (2.37)) can be written in the form

$$\frac{\partial u_j}{\partial t} + u_j \frac{\partial u_j}{\partial r} - \delta_u \frac{v_j^2}{r} - f v_j = -\frac{\partial \phi_j}{\partial r} - \Phi_j + F_{rj} + \cdots \tag{1}$$

$$\frac{\partial v_j}{\partial t} + u_j \frac{\partial v_j}{\partial r} + \delta_v \frac{u_j v_j}{r} + f u_j = F_{\lambda j} + \cdots , \tag{2}$$

where u_j, v_j, are the radial and azimuthal wind components in layer-j, $(\partial \phi_j / \partial r) + \Phi_j$ is the radial pressure gradient, and F_{rj} and $F_{\lambda j}$ are the frictional terms in the radial and azimuthal directions. The quantities δ_u and δ_v are switches: when $\delta_u = 1$ and $\delta_v = 1$, we recover the original equations of DP88; when $\delta_u = 0$ and $\delta_v = 0$, the nonlinear terms are those of the slab-symmetric version. Similarly, Eq. (3.3) of DP88, the mass continuity equation, is

$$Q_{3/2}^{-} - Q_{3/2}^{+} = (H_1 + h_1) \left(\frac{\partial u_1}{\partial r} + \delta_{\text{conv}} \frac{u_1}{r} \right) \tag{3}$$

when $\delta_{\text{conv}} = 1$. When $\delta_{\text{conv}} = 0$ we obtain the slab-symmetric version.

(*d*) *Angular-momentum versus linear-momentum conservation*

In the first intermediate case, we investigate the importance of angular-momentum conservation for the intensification, by setting both δ_u and δ_v equal to zero*, but keeping $\delta_{\text{conv}} = 1$. In this case the vortex does not intensify. The time–radius plots resemble the slab case, even though terms on the right-hand side of Eqs. (1) and (2) have their axisymmetric form. We do not show the results of this case. As an intermediate calculation we show in Fig. 4(a) the evolution of the azimuthal wind for the case

* Examination of the kinetic-energy equation formed from Eqs. (1) and (2), shows that unless $\delta_u = \delta_v$, the formulation would lead to spurious energy sources in the system.

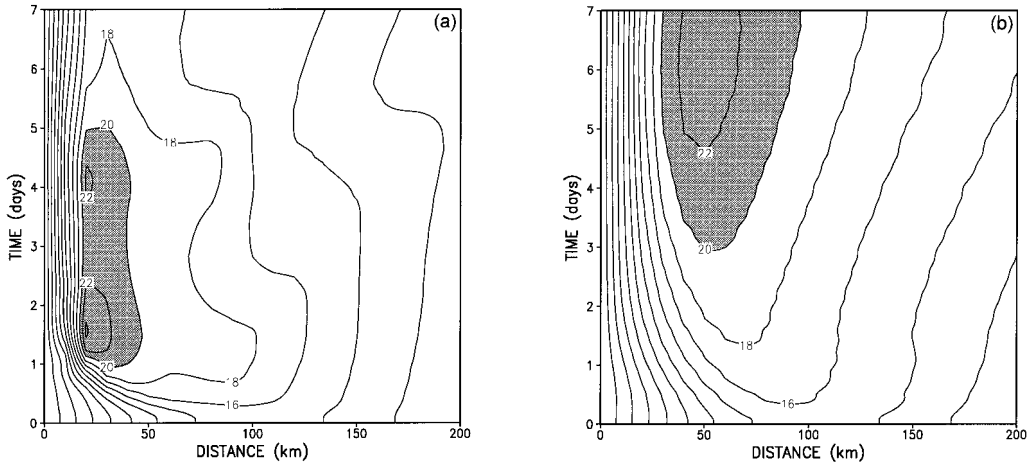

Figure 4. Isotachs of azimuthal wind speed for two intermediate cases: (a) $\delta_u = 0.5$, $\delta_v = 0.5$ and $\delta_{\text{conv}} = 1$; (b) $\delta_u = 1$, $\delta_v = 1$ and $\delta_{\text{conv}} = 0.85$. Contour interval is 2 m s^{-1} with values larger than 20 m s^{-1} shaded.

$\delta_u = \delta_v = 0.5$. There is clearly less intensification than in the axisymmetric case, but the plot shows a greater resemblance to that case (cf. Fig. 2(a)) than to that for the slab-symmetric case. As expected, as δ_u and δ_v are increased beyond 0.5, the solution approaches that for the axisymmetric case.

(*e*) *Axisymmetric versus slab convergence*

Setting $\delta_{\text{conv}} = 0$ with $\delta_u = \delta_v = 1$ is equivalent to using the convergence from a slab boundary layer to calculate the $Q^+_{3/2}$. The vortex in the calculation with these values does not intensify and even when δ_{conv} is increased to 0.5, there is only slight intensification. In contrast, significant intensification occurs when $\delta_{\text{conv}} = 0.85$ (see Fig. 4(b)), suggesting that vortex intensification in the calculations using the representation of convection in model-1 is sensitive to the precise amount of convective heating.

(*f*) *Model-2 and other convection schemes*

A limitation of the foregoing calculations is the use of a convection scheme in which the rate of convective heating is tied to mass convergence in the boundary layer. Therefore, as shown above, the geometrical differences between the axisymmetric and slab-symmetric versions of the model lead to a difference in the rate of convective heating as well as the different surface wind speed resulting from angular-momentum conservation. To check that the larger rate of convective heating in the axisymmetric model is not the decisive factor leading to development in the axisymmetric model, we carried out additional calculations using model-2, using a range of closures on the cloud-base mass flux of deep convection. Figure 5 summarizes the results of the six experiments using the new model, three using the axisymmetric version with one of the closures for deep convection, and three using the slab-symmetric version with each closure. The calculations assume the same initial vortex as before and the initial thermal and moisture structure is the same as that used by Nguyen *et al*. (2002), which is slightly stable to deep convection at the initial instant. The figure shows the maximum wind speed in the boundary layer in each calculation as a function of time. As in the earlier calculations, the vortices in the axisymmetric calculations all grow, while those in the slab-symmetric case do not show any sustained development. It is interesting to note

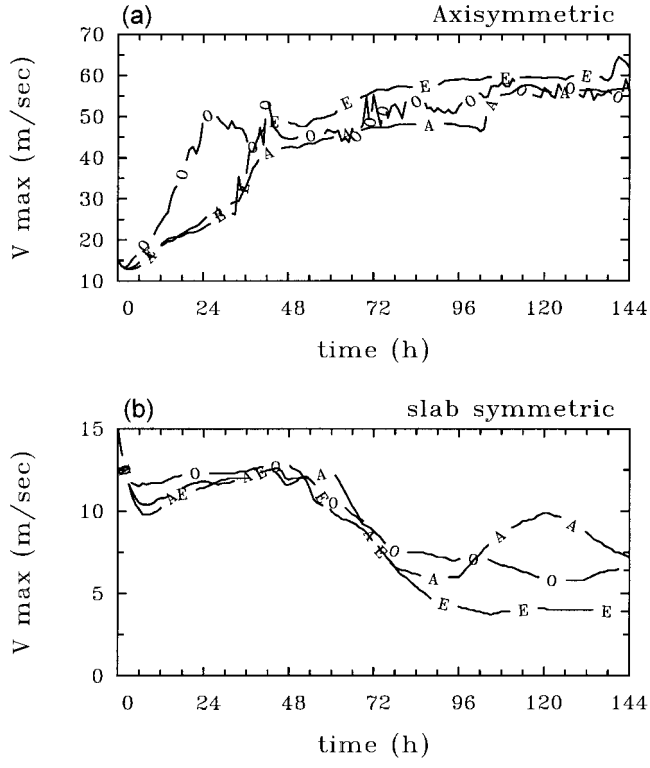

Figure 5. Maximum azimuthal/transverse wind speed in (a) an axisymmetric and (b) a slab-symmetric version of the minimal three-level model of Nguyen *et al*. (2002). The symbols A, E and O mark the curves for the modified forms of Arakawa, Emanuel and Ooyama closures for deep-convection parametrizations.

that with the Ooyama scheme, the period of rapid development occurs earlier in the axisymmetric case compared with the other two schemes, suggesting that, at least for the parameters chosen, this scheme produces the maximum convective heating.

(*g*) *Stronger initial disturbance in the slab-symmetric case*

One might ask whether the disturbance in the slab-symmetric case could grow if the initial disturbance were sufficiently large. To answer this question we carried out additional calculations with the slab-symmetric versions of both models, the results of which are summarized in Fig. 6. Panel (a) of this figure shows time series of the maximum tangential wind speed in layer-2 for six calculations using model-1. These include the standard calculation described in section 4(b), two calculations in which the strength of the initial vortex was increased to 25 m s^{-1} or 35 m s^{-1}, and three more in which the radius of maximum tangential wind speed was increased from 100 km to 150 km. Panel (b) of Fig. 6 shows the corresponding calculations using model-2 with the Arakawa scheme for convection. In all these calculations, following a brief period of transient growth, all the disturbances decay. Thus, it does not appear possible for the two-dimensional disturbance to grow spontaneously, even from a relatively (and possibly unrealistically) strong initial perturbation.

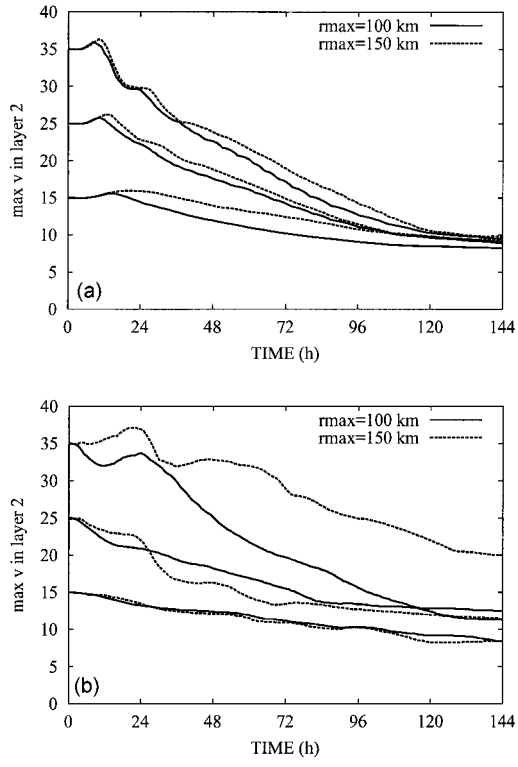

Figure 6. Time series of the maximum tangential wind speed in layer-2 for six calculations using the slab-symmetric version of each model with an initial vortex strength of 15, 25, or 35 m s^{-1}, and an initial radius of maximum tangential wind speed (rmax) of either 100 km (solid curves) or 150 km (dashed curves): (a) model-1, (b) model-2 with the Arakawa scheme for convection.

5. Discussion

We attribute the quantitative differences between the axisymmetric and slab-symmetric calculations to two geometrical effects: the first associated with the conservation of absolute angular momentum, and the second associated with the boundary-layer convergence.

In the axisymmetric model, the absolute angular momentum is defined by $rv + (fr^2/2)$, while in the slab-symmetric model it is defined by $v + (fx/2)$. Thus, an air parcel in the axisymmetric model which arrives at radius r from a larger radius r_0, conserving its angular momentum, will have a tangential velocity $v = \{v_0 + (fr_0/2)\}(r_0/r) - (fr/2)$, where $v_0 = v(r_0)$, whereas an equivalent air parcel in the slab-symmetric model will have a transverse velocity $v = \{v_0 + (fx_0/2)\} - (fx/2)$. The factor r_0/r in the axisymmetric model implies that a much larger wind speed can be attained as r decreases than in the slab-symmetric model as $|x|$ decreases. As a result, much larger surface fluxes of latent heat are possible in the former case. This is confirmed by a comparison of the evolution of the surface heat flux as a function of r or x and time in the two models shown in Figs. 2(c) and 3(c). The pattern of the moisture flux in the slab-symmetric case reflects the distribution of u (not shown), as the transverse component v has less structure. The increased moisture flux elevates the degree of deep convective instability as characterized by the parameter η.

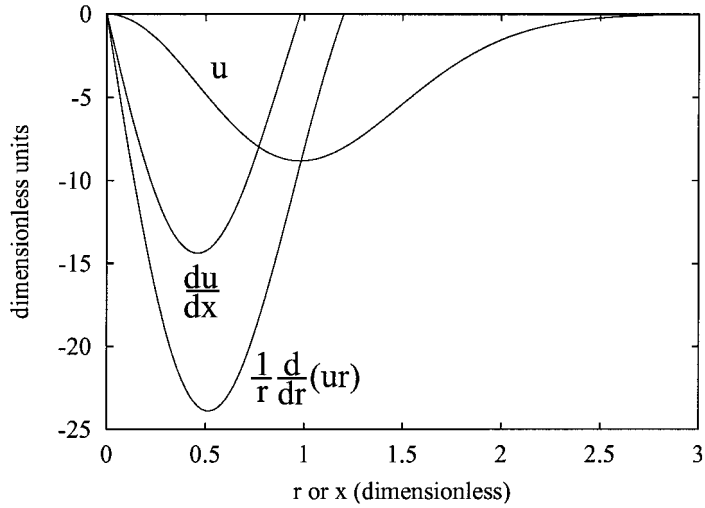

Figure 7. Convergence in the axisymmetric ($(1/r)\,\mathrm{d}(ur)/\mathrm{d}r$) and slab-symmetric ($\mathrm{d}u/\mathrm{d}x$) versions of the model for an idealized radial inflow (u) profile. Units are non-dimensional.

The importance of the $(1/r)$-type dependence of v implied by angular-momentum conservation for development in the axisymmetric case is highlighted by the calculation where the slab-symmetric conservation law is used in the axisymmetric model (see subsection 4(d) above). In this extreme calculation, development does not occur, but it begins as the terms involving δ_u and δ_v in Eqs. (1) and (2) are progressively increased.

The second effect of differing geometry is that, for the same radial/lateral profile of boundary-layer inflow, the convergence in the axisymmetric case, $(1/r)\,\mathrm{d}(ru)/\mathrm{d}r$, is about twice as large as in the slab-symmetric case, $\mathrm{d}u/\mathrm{d}x$, on account of the additional term $1/r$. This difference is indicated in Fig. 7 for a representative inflow profile. The larger convergence means that for the convergence-based closure on deep convection used in the model, the rate of cumulus heating would be approximately twice as large in the axisymmetric case, even if the inflow profile and the distribution of η were the same. In fact, the inflow is larger in the axisymmetric case, as are the values of η, because of the increased surface fluxes of latent heat. Thus both effects combine to produce a much stronger disturbance than in the slab-symmetric case. It is clear from the intermediate case discussed in subsection 4(e) that the foregoing geometrical factors are not independent when using the convective parametrization scheme of model-1. Indeed the amount of convective heating required for development in the axisymmetric case is not significantly less than that present in the calculation of subsection 4(a).

Calculations using model-2 show that, even in cases where the deep convective mass flux is not coupled with the convergence, development does not occur in the slab-symmetric case. Except for the fact that there is a brief period of weak development using the Ooyama scheme in the slab-symmetric version of model-2, the calculations using this model support the results obtained using model-1.

6. Conclusions

We have shown that there are important quantitative differences between the evolution of a hurricane-like disturbance in an axisymmetric model and that of a disturbance with a similar initial structure in the corresponding slab-symmetric model. Because of a

geometrical factor, conservation of absolute angular momentum for inward-moving air in the axisymmetric model permits much larger tangential wind speeds to be obtained than in the slab-symmetric model. As a result, the sea-surface latent-heat flux, which is wind-speed dependent, is much larger in the axisymmetric model, and provides a larger energy supply to the storm per unit area.

In the axisymmetric version of the model, the boundary-layer convergence is much stronger than in a slab-symmetric version and with a convergence-based closure on deep convection, the deep convective heating is much stronger. Nevertheless, calculations using non-convergence-based closures in model-2 show that this is not the overriding effect in producing development in the axisymmetric case. It follows that the slab-symmetric model in general does not provide a dynamically equivalent surrogate for the corresponding axisymmetric configuration and, therefore, for a hurricane.

ACKNOWLEDGEMENTS

We are grateful to Dr Michael Montgomery and an anonymous reviewer for their constructive suggestions on an earlier version of the manuscript. This research was supported by the US Office of Naval Research through Grant No. N00014-95-1-0394.

APPENDIX

The model formulation differs from that of DP88 as follows:

1. First we note that there are misprints in DP88 in Eq. (3.1). The term in parentheses should read: $r(\partial/\partial r)$. In Eq. (2.31) the overbar must be switched: $(S_j - \overline{S}_j)$ and in Eq. (3.12) the factor in front of the second term on the right-hand side must read: $M_3 - M_2/P_{3/2} - P_{7/2}$.

2. The proportionality constant η is calculated as in DP88 Eq. (3.11), but the moist static energy in layer-1 is

$$\Lambda_1 = M_1 + Lq_1. \tag{A.1}$$

3. Following Shapiro (1992), the drag coefficient for the surface momentum flux is taken to be

$$C_{\mathrm{D}} = (1.024 + 0.05366 R_F|\mathbf{u}|) \times 10^{-3} \tag{A.2}$$

where $R_F = 0.8$ is a wind-speed reduction factor. Here we set $C_{\mathrm{E}} = C_{\mathrm{D}}$.

4. We use the same horizontal diffusivity $\lambda = 1000\ \mathrm{m^2 s^{-1}}$, and vertical diffusivity, $\mu = 5.0 \times 10^{-5}\ \mathrm{m^2 s^{-1}}$, as DP88. A bi-harmonic filter term is chosen with coefficient $\lambda_4 = 4.63 \times 10^{10}\ \mathrm{m^4 s^{-1}}$, which corresponds to a damping time of 60 h.

5. An attempt to reproduce the DP88 control simulation (their Fig. 2) showed some sensitivity to details of the numerical scheme. The scheme used is described briefly below.

The solution method uses finite differences. Although the accuracy of finite differences is less than that of spectral methods using standard schemes, the method is more versatile and the desired accuracy can be achieved by increasing the resolution. Another advantage is the subdivision into finite volumes with an appropriate choice of staggering. The radial and tangential wind components, u and v, are calculated at regular radial locations starting at $r = 0$, where $u = 0$ and $v = 0$. All other quantities including the 'Q's are calculated at intermediate locations. In the experiments shown, we use 100 grid points with intervals $\Delta r = 10$ km. This represents a higher resolution than used

by DP88 and enables the vortex 'eye' region (the region of subsidence surrounding the axis) to be better resolved.

For time integration we adopted the standard Adams–Bashforth third-order method. The finite differencing has a substantial impact on the results. Most crucial is the method for evaluating the divergence in layer-1. The only method which was found to have a stable behaviour was when the divergence was calculated from its immediate neighbours:

$$\left(\frac{1}{r}\frac{\partial}{\partial r}(ru_1)\right)_{i+1/2} = \frac{1}{r_{i+1/2}}\frac{r_{i+1}u_{i+1} - r_i u_i}{\Delta r}. \tag{A.3}$$

We have investigated various ways to evaluate the advection terms, among them a fourth-order accurate advection scheme and the flux form of Eqs. (2.36)–(2.38). However, the hoped for superiority was not obtained when the additional terms involving the 'Q's were included.

We found a somewhat slower development of the vortex than reported in DP88 if all parameters, including the domain size and resolution, are the same as in DP88. All parameter dependencies are qualitatively the same as reported by DP88. We obtained the best quantitative agreement using 64 intervals for the control experiment, whereas DP88 use a Bessel series truncated at $N = 32$. This confirms the general rule that n spectral modes are 'worth' $2n$ grid points.

There is a difference in the rate of vortex evolution depending upon whether convective instability is allowed to accumulate, or whether it is rapidly removed. The time-scale for the convective adjustment to occur in the present model is simply the time step, rather than a specified time-scale for convection. Taking a finer resolution requires a smaller time step, which speeds up vortex development. A primary factor governing the evolution of the initial vortex to hurricane strength is the horizontal resolution.

6. We use a third-order upstream advection scheme. This scheme is not positive definite like the standard upstream method, although oscillations are weak compared with centred schemes, and amplitudes are comparable to them. The beneficial effect of the bi-harmonic damping term is in filtering out such oscillations.

7. The initial vortex profile is given by the function of $s = r/r_{\max}$ or $s = x/x_{\max}$:

$$v = 1.7880321\, v_{\max}\frac{\{1 + 3a(\chi s^2)^2\}s}{\{1 + (\chi s^2)^2 + a(\chi s^2)^3\}^2}, \tag{A.4}$$

where r or x measure distance from the axis and $v_{\max} = 15$ m s^{-1}, $r_{\max} = x_{\max} =$ 100 km, $\chi = 0.3398057$, and $a = 0.0137047$.

8. The treatment of the outer boundary for the radial velocity component u requires care. Gravity waves may travel far outward with little loss in amplitude and be reflected at the outer boundary, eventually triggering sporadic deep convection. This may be a problem unless the domain size is very large. Here we implement a radiation boundary condition suggested by Miller and Thorpe (1981). A further improvement is to include a damping term in the right-hand side of the tendency equation for u_j, and v_j.

$$\frac{\partial}{\partial t}u_j = \ldots - du_j \quad \frac{\partial}{\partial t}v_j = \ldots - dv_j, \tag{A.5}$$

where the damping term $d(r) = d_{\max}(1/2)[1 + \cos\{\pi(r - r_{\rm d})/(r_{\rm b} - r_{\rm d})\}]$ when $r \geq r_{\rm d}$, where $r_{\rm b}$ is the maximum radius in the model, and $r_{\rm d}$ is the radius where damping starts to become active. In the calculations we used $d_{\max} = 1/\tau$, $\tau = 1h$, $r_{\rm d} = (3/4)r_{\rm b}$. The damping terms reduce the activity of the flux terms at large radii. We assume that

the equations for u_j reduce to an advection equation with advection speed c and a damping term of the form

$$\frac{\partial}{\partial t}u + c\frac{\partial}{\partial r}u = -du. \tag{A.6}$$

The Miller–Thorpe procedure is not suitable for v because this component is tangential to the boundary. Instead we include the foregoing damping term, so that the equation to be solved instead of Eq. (2.37) is

$$\frac{\partial}{\partial t}v_j + fu_j = -dv_j. \tag{A.7}$$

The layer thickness at the outer boundary is obtained on the assumption of geostrophic balance based on DP88 Eq. (2.36) and ignoring the small term Φ_j therein. We found that a zero-gradient condition for the boundary-layer mixing ratio, q_1, at the outer boundary condition was adequate.

REFERENCES

Arakawa, A. 1969 'Parameterization of cumulus convection'. Pp. 1–6 in Proceedings of the WMO/IUGG symposium on numerical weather prediction, 26 November–4 December 1968, Tokyo. Japan Meteorol. Agency IV, **8**

Charney, J. G. 1973 Planetary fluid dynamics. Pp. 331–344 in *Dynamical meteorology*. Ed. P. Morel. Riedel

Charney, J. G. and Eliassen, A. 1964 On the growth of the hurricane depression. *J. Atmos. Sci.*, **21,** 68–75

DeMaria, M. and Pickle, J. D. 1988 A simplified system of equations for simulation of tropical cyclones. *J. Atmos. Sci.*, **45,** 1542–1554

Emanuel, K. A. 1995 The behavior of a simple hurricane model using a convective scheme based on subcloud-layer entropy equilibrium. *J. Atmos. Sci.*, **52,** 3960–3968

Emanuel, K. A., Neelin, J. D. and Bretherton, C. S. 1994 On large-scale circulations in convecting atmospheres. *Q. J. R. Meteorol. Soc.*, **120,** 1111–1143

Miller, M. and Thorpe, A. 1981 Radiation condition for the lateral boundaries of limited-area numerical models. *Q. J. R. Meteorol. Soc.*, **107,** 615–628

Nguyen, C. M., Smith, R. F., Zhu, H. and Ulrich, W. 2002 A minimal axisymmetric tropical cyclone model. *Q. J. R. Meteorol. Soc.* in press

Ooyama, K. 1969 Numerical simulation of the life cycle of tropical cyclones. *J. Atmos. Sci.*, **26,** 3–40

1982 Conceptual evolution of the theory and modelling of the tropical cyclone. *J. Meteorol. Soc. Jpn.*, **60,** 369–379

1997 'Footnotes to conceptual evolution'. Pp. 13–18 in Preprints of the 22nd conference on hurricanes and tropical meteorology, 19–23 May 1997, Ft. Collins, Colorado, USA. American Meteorological Society, Boston

Shapiro, L. J. 1992 Hurricane vortex motion and evolution in a three-layer model. *J. Atmos. Sci.*, **49,** 140–153

Smith, R. K. 1997 On the theory of CISK. *Q. J. R. Meteorol. Soc.*, **123,** 407–418

Smith, R. K., Ulrich, W. and Dietachmayer, G. 1990 A numerical study of tropical cyclone motion using a barotropic model. Part I: The role of vortex asymmetries. *Q. J. R. Meteorol. Soc.*, **116,** 337–362